CHAPTER 2

Star formation beyond the optical boundaries-XUV disks in distant dwarfs

2.1 Introduction

In 2005, with the help of *GALEX* observations, Gil de Paz & Madore[318] and Thilker et al.[319] discovered ultraviolet (UV) emission beyond the optical extents in the galaxies NGC4625 and M83. This UV emission generally emanates from bright star-forming complexes in the far outskirts of the galaxies which contain young and massive OB-type stars [18, 31]. Galaxies exhibiting such spatially extended UV (hereafter XUV) emission/star formation are called XUV disk galaxies. Studies have shown that XUV disks could reach 3-4 times the optical extents of the galaxies [18, 318]. It is seen that XUV behaviour is a common evolutionary phenomenon in, but not restricted to, star-forming spiral galaxies [2, 18, 319]. Early-type galaxies have also shown outer disk star formation [320–324] and in fact a large XUV disk survey by Lemonias et al. [2] suggests that they are more likely to be found in these early galaxies. The survey also shows that on average, at least 4-14% of galaxies up to z$\simeq$0.05 are seen to host XUV disks.

Emission in XUV disks usually trace their large gas reservoirs but at the same time, star-formation efficiencies are low[18, 325–327]. Their origins lie at interaction events that perturb the smooth and extended gas disk [2, 18]. On the other hand, gas infall from the IGM via filaments[73, 328, 329] might also trigger such outer star formation.

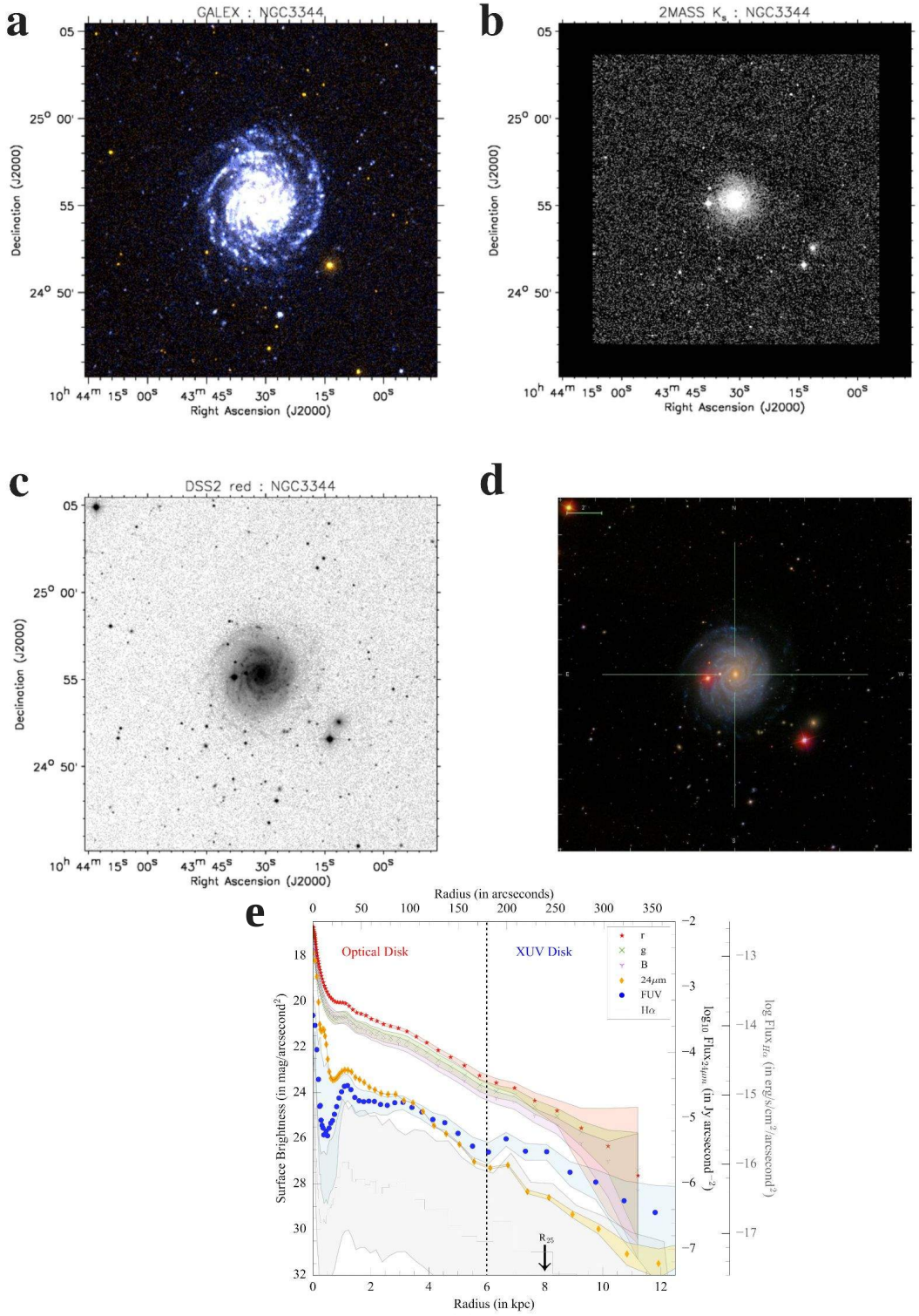

Figure 2.1: **Example of XUV disk galaxy: NGC 3344[18]. a**: *GALEX* FUV and NUV composite image with its bright star forming regions spanning a large area. **b**: NIR imaging in 2MASS K_s band. **c**: A Digital Sky Survey (DSS) image in the red channel and **d**: RGB composite with *SDSS* g (blue), r(green), i(red) bands. Credit: Thilker et al. 2007 [18]. This is a Type 1 XUV disk as per Thilker et al. 2007. We discuss the Thilker et al. 2007 classification later in the chapter. **e**: Multi-band surface brightness profiles of NGC3344 (Credit: Padave et al. [330]). It shows the inner optical and XUV disk of the galaxy.

2.2 Motivation

The discovery of XUV disks provided ample insight into the assembly history and build-up of galaxy disks. For example, XUV disks may evolve to produce[331] anti-truncated or up-bending (Type III) disk profiles in galaxies, such as that in NGC 2967[332, 333] (later in Figure 2.3). Nearby dwarf galaxies are also seen to exhibit such light profiles[5, 334]. XUV disks are considered to be indicators of inside-out formation of galactic disks[335–340]. This scenario of inside-out formation has been predicted by semi-analytic models where the galactic disks must be forming their inner regions first and then the outer parts, to reproduce the observed size–luminosity–velocity relations[341, 342]. Several studies mounting to observational evidence on the inside-out scenario have been done in the past[343–352]. However, local group of dwarf galaxies have indicated a contrary scenario[27]. On the other hand, high redshift (z$\sim$2) dwarf galaxies have shown an inside-out assembly signature[353]. Therefore, we need to look into these galaxies when they are still in their formative stages and understand the origin of this dichotomy. It is interesting to note that Lemonias et al. 2011[2] have indicated the existence of XUV disks in low-mass galaxies in the nearby Universe.

2.3 Sample and Data

We selected a sample of Blue Compact Dwarf galaxies (BCDs), described below, from the *GOODS-South* field for which we acquired high-quality multi-wavelength observations. Recently the *GOODS-South* field has been observed by the *Ultra-Violet Imaging Telescope (UVIT)*[6] onboard *AstroSat*[7] in the far-ultraviolet (FUV) and near-ultraviolet (NUV) (P.I. Kanak Saha, Saha et al. *in preparation*). The novelty of these observations is the unprecedented spatial resolution (three times better than *GALEX*) and depth (3σ mag_{FUV} = 27.9 [107]) of the data in this wavelength range ($\sim$1300 - 3000 Å). The even higher resolution FUV observations from *HST* were limited by coverage. Such deep and high-resolution UV observations motivate us to investigate the low-density star formation in the faint outskirts of galaxies.

2.3.1 Blue Compact Dwarf galaxies

BCDs are often considered as a star-forming phase in dwarf galaxy evolution (e.g. [116, 118, 121, 248]). As introduced in Chapter 1, these are low-luminosity, $M_K > -21$ mag[3], metal-deficient ($\frac{1}{50}$ $Z_\odot \leq Z \leq \frac{1}{2}$ $Z_\odot$)[4] and star forming (10^{-3} - 10^2 $M_\odot$ yr^{-1})[249] dwarfs characterized by their intense central star formation[250] in the Local Universe. Also, their characteristic, underlying old stellar disk[20, 120] - often referred to as the host could have formed over a series of star-formation episodes which in turn also regulate further star formation[26, 120, 248, 267, 268]. Young star-forming sites - younger than the central starburst ($\leq$10 Myr), have been detected in the outskirts of BCDs as well[354]. At the same time simulations of BCD formation[282] via gas-rich dwarf mergers have shown extended gaseous disks. Hence it is plausible to expect stars to form in these outskirts.

2.3.2 AstroSat observations and other archival data

We select our sample BCDs using the following criteria[3] - (i) central surface brightness < 22 mag arcsec^{-2} in *HST* F435 filter; (ii) rest-frame $B - R < 1.0$; (iii) stellar mass $< 10^9$ $M_\odot$ and redshift $z < 0.25$ (obtained from Skelton et al. 2014[298]). The surface brightness dimming effect has been taken into consideration while applying the above criteria. These criteria select only 14 BCDs [355] in the entire *GOODS-South* field. The observed field using *AstroSat UVIT* is shown in figure 2.2.

In this study, we primarily make utilize archival observations from *HST* [300], *HAWK-I* [305] along with new UV observations from *UVIT*. We use the official L2 pipeline to process the orbit-wise *UVIT* dataset[107] of the *GOODS-South* field (P.I. Kanak Saha, ID: GT05-240). We remove the cosmic-ray affected frames accordingly which resulted in a $\sim$ 15% data loss in the final science-ready images and the subsequent photometry estimates. In addition, there was data loss owing to the mismatch in the time-stamp on the VIS (visual) filter and FUV (F154W) or NUV (N242W) filters. The final science-ready images had a total exposure time of about 17.7 and about 17.3 h in F154W and N242W, respectively [107].

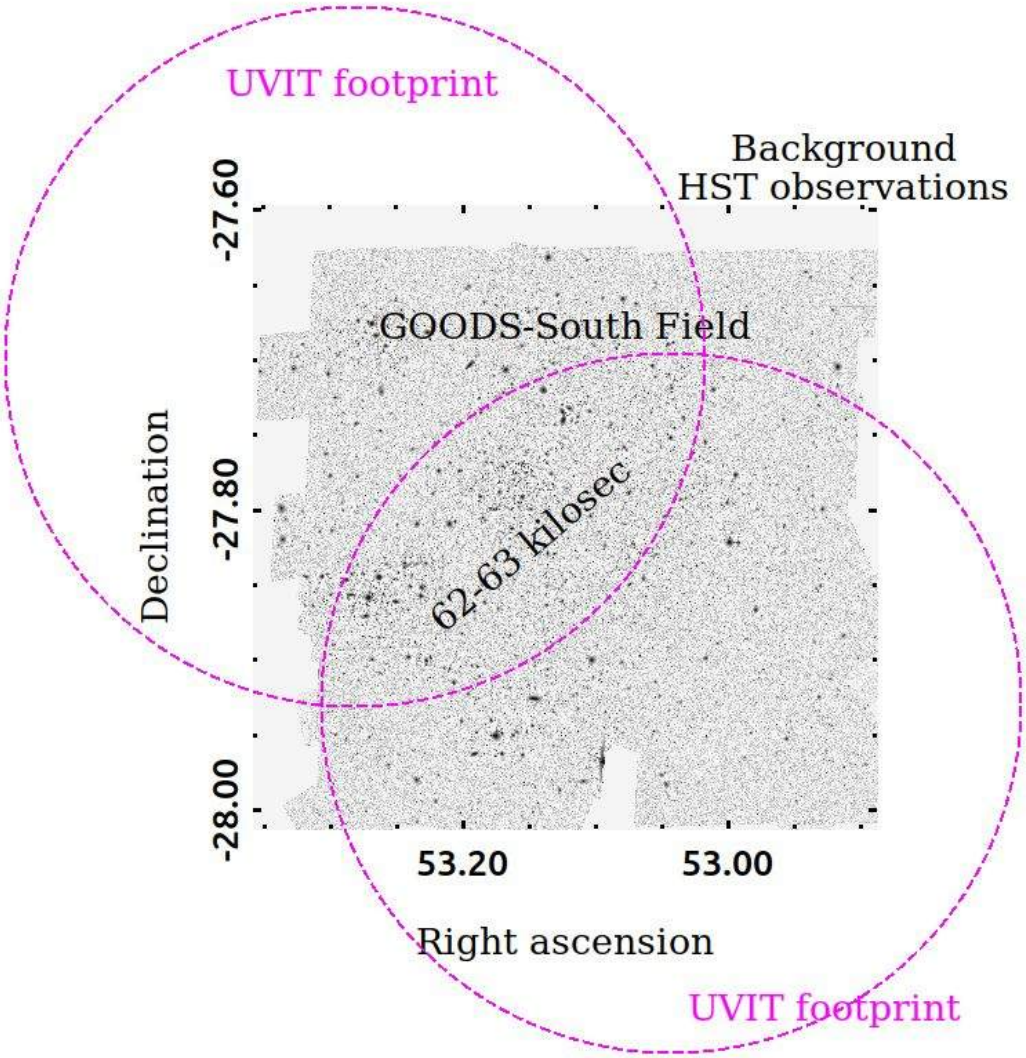

Figure 2.2: **AstroSat UV Deep Field South** Observed regions of the *GOODS-South* field using *UVIT* shown in magenta dashed circles. Proposal ID: GT05-240, P.I. Kanak Saha (More information on AUDF[a]). The background image is HST imaging from the Hubble Legacy Fields archive[b][300]

[a] audf.iucaa.in/
[b] https://archive.stsci.edu/prepds/hlf/

2.4 Data Analysis

2.4.1 Characterising the UVIT observations

2.4.1.1 Background estimation

We employ the following procedure to estimate the sky background. We run *Source Extractor*[21] (*SExtractor*) with a low minimum detection threshold

on the parent *UVIT* image. We dilate the obtained segmentation map so that we can mask the outer faint emission from all the detected sources. We then created a flux histogram by placing a large set of boxes of size 9 pixels randomly over the masked image. We also visually inspect the placement of the boxes to avoid the masked regions. We use a Gaussian function to fit the resulting histogram whose mean is the estimated background. The FUV and NUV sky surface brightness comes out to be 28.43 ± 0.01 mag arcsec^{-2} and 27.6 ± 0.003 mag arcsec^{-2} respectively. The 3σ (5σ) limiting point source magnitude within an aperture of radius 1" is ∼27.94 (27.44) mag and ∼28.17 (27.62) mag in the FUV and NUV respectively. The local sky can vary from location to location. So, to estimate the local background level for each BCD, we follow the same procedure on individual 101×101 pix cutouts. We do this because accurate background estimation is essential for accurate photometry of faint structures in the outer parts of galaxies. We use the same galaxy IDs for our BCDs as in Lian et al. 2015[355] for a one-to-one comparison.

2.4.1.2 Point Spread Function estimation

We select bright FUV, and NUV stars from the *GOODS-South* field to characterize the Point Spread Function (PSF) of the *UVIT* observations. In the case of FUV we use a single bright star (17.8 mag), whereas in the NUV, we select six stars (19.5-18.4 mag). We choose them such that they are sufficiently isolated and the core is free from contamination from companions. We carefully clean away nearby objects and stack the stars (in the case of NUV) to obtain a representative star. Then we use the IRAF[308] ELLIPSE task [307] to obtain 1D PSF profiles. To model the instrumental PSF, we use a combination of Moffat[356] profile (for the core) and an exponential (for the outer wing)[357–359]. It is given by:

$$I_{PSF}(r) = I_{c0}\left[1 + \left(\frac{r}{\alpha}\right)^2\right]^{-\beta} + I_{w0}\, e^{-r/R_s}, \tag{2.1}$$

where the first term represents the Moffat component and symbols have their standard meaning; R_s denotes the scale-length of the exponential profile, I_{w0} is the extrapolated central intensity of the wing component. The full width

half maximum (FWHM) is given as:

$$FWHM = 2\alpha\sqrt{2^{1/\beta} - 1}, \tag{2.2}$$

Using equation 2.1 we perform a least squares fit to the observed 1D profiles of the *UVIT* PSFs. The F154W (FUV) and N242W (NUV) PSF FWHMs are ∼1.4 arcsec and 1.3 arcsec respectively - which is more than 3 times better resolution than the *GALEX* UV deep field [360].

All measured magnitudes have been corrected for Galactic extinction[361] using a E(B−V) = 0.008 mag towards the *GOODS-South* field[362]. We use $\frac{A_\lambda}{E(B-V)}$ = 8.06 and 7.95 for FUV and NUV passbands respectively[363].

2.4.2 Multiband surface photometry

We use the IRAF[308] ELLIPSE[307] task and fit elliptical isophotes to the BCDs in the background-subtracted images of *HST* F435W band. We take care to mask all nearby sources around each BCD before performing surface photometry. We keep a fixed centre when fitting isophotes to the BCDs in the F435W band images. We proceed to obtain the surface brightness profiles (SBPs) as follows. The intensity (I in units of counts/s/pix) at a semi-major axis length (SMA) r is obtained by measuring the total flux within an annulus of SMA r and $r + \Delta$r and then dividing this value by the total number of pixels within that annulus. Here, Δr = 4 pixels = 0.24" in *HST* imaging. We correct the intensity (I) for redshift dimming by a factor of (1+z)^4. The surface brightness (μ) at a given SMA is then given by

$$\mu = -2.5 \log \frac{I}{pixel\ scale^2} + magZP \tag{2.3}$$

The fitted isophotes in the F435W band imaging are then used to extract the SBPs in the F154W, N242W and F160W bands. We varied Δr from 0.48" (inner regions) to 1.44" (outer parts) so that we can avoid a sub-pixel sampling in the inner parts of the *UVIT* images (*UVIT* plate scale = 0.417"). This allows

us to have a large enough area in the outer parts (comparable to FUV PSF ∼1.4") to collect sufficient signal that has been affected by the *UVIT* PSF.

The photometric zeropoints[6, 300], magZP are 17.78 (F154W), 19.81 (N242W), 25.68 (F435W), and 25.94 (F160W). The surface brightness errors ($\Delta\mu$) are estimated by using the background sky rms within each annulus as follows:

$$flux\ error = \sqrt{n_{pix}\sigma^2_{sky} + \frac{flux}{exptime}}\ \ and\ \ \Delta\mu = \frac{flux\ error}{flux}\frac{2.5}{\ln 10} \tag{2.4}$$

Here n_{pix} denotes the number of pixels within each annulus, flux and exptime refer to the total counts/s within the annulus and total exposure time respectively. The *HST* images came along with their associated weight images which we use to compute the sky rms, σ_{sky}. The median values of locally obtained σ_{sky} are 6.41×10^{-6} (F154W) and 3.54×10^{-5} (N242W) counts/s/pix. These correspond to limiting surface brightness levels of 29.6 (FUV) and 29.7 (NUV) mag arcsec^{-2} at 3σ above the background in an aperture of radius equal to PSF FWHM.

Outer extent of a galaxy: For each 1D SBP, we obtain 1D S/N profile for each galaxy and use a S/N =3 criteria to mark their extent in any band. We further correct the extent for the effect of the PSF as follows:

$$r_{corr} = \sqrt{r^2_{obs} - hwhm^2} \tag{2.5}$$

where r_{corr} is the corrected extent, r_{obs} is the observed extent at which S/N = 3, and hwhm is the half-width at half-maximum in a passband. We correct all the extents quoted in the text for the PSF as explained above.

2.4.3 Modelling the surface brightness profiles

Most disk galaxies including dwarfs follow intrinsic exponential profiles[334]. We use *PROFILER*[310] to model the *HST* SBPs with a combination of Sersic and exponential or a single exponential [355] function. The disk SBPs can be

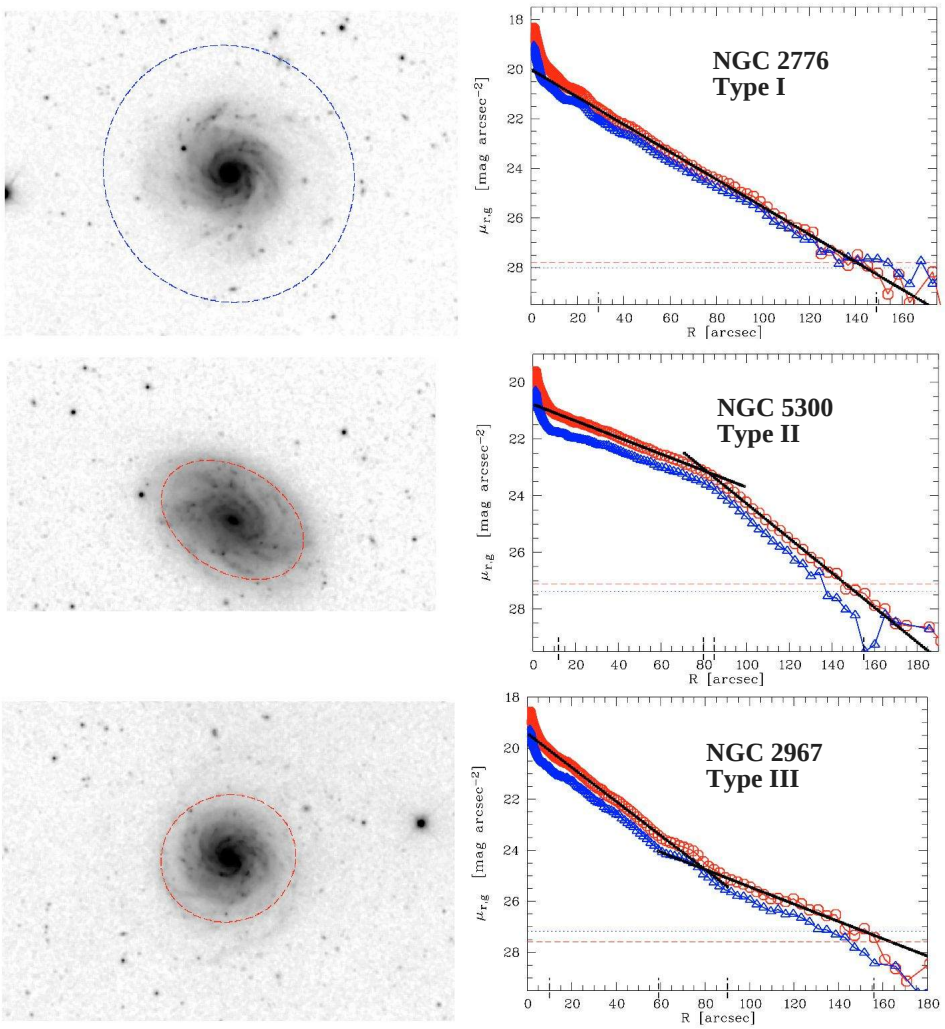

[333].

Figure 2.3: **Three classes of exponential surface brightness profiles.** *Left* : *SDSS* r'-band galaxy images. The ellipses mark the break in the surface brightness profiles in the right. For Type I profile the blue ellipse marks the limiting surface brightness level. *Right* : The surface brightness profiles in the *SDSS* g' (blue triangles) and r' (red circles) bands. The black lines are fits to the profile in r'-band. The horizontal blue and red curves mark the critical surface brightness in respective bands. Further details can be found in Pohlen & Trujillo 2006

broadly classified into three types - Type-I, Type-II and Type-III[332, 333, 364]. Type-I refers to a regular exponential profile whereas Type-II and Type-III are truncated with either a down-bending or up-bending trend. Example for each class of profile is shown in Figure 2.3. So, we also consider truncated exponential profiles in addition to Sersic plus exponential, to obtain a more realistic modelling of the BCDs in the *HST* images. We model the UV disk with a different approach because *PROFILER*[310] does not consider error bars during the fitting. In our simplistic approach, we consider a pure exponential 2D

model in both the *UVIT* bands that will have the same ellipticity as that of the outermost fitted isophote (having S/N $\geq$ 3) in the *HST*/F435W band. We do not use truncated exponential disks because given the resolution and angular size of the galaxies, we cannot confirm or deny their existence. We find that the galaxies appear fairly face-on in the HST images. So we do not consider inclination effects in the 2D models. We then convolve the 2D exponential disk with the respective *UVIT* PSFs and create model UV disks. We then obtain 1D SBPs of the models with the same ellipse geometric parameters as used for UV surface photometry. We perform least-squares optimization using the MPFIT routine[365], which is an implementation of the MINPACK[366] Levenberg-Marquardt nonlinear least-square optimization algorithm, to fit the 1D model profiles to the observed ones. This provides us with the intrinsic UV scale-lengths and central surface brightnesses of the BCDs.

2.4.4 Measuring UV light beyond the optical extent

We measure the fraction of intrinsic FUV light in the XUV region (defined by the region bound by S/N = 3 extents, obtained as per equation 2.5, in the optical and FUV) denoted by ΔL_x:

$$\Delta L_x = \frac{L_{x,FUV} - L_{x,opt}}{L_{x,FUV}}, \tag{2.6}$$

Here $L_{x,FUV}$ is the intrinsic light within the FUV extent ($R_{out,FUV}$), and $L_{x,opt}$ is the light within the optical extent blurred by the *UVIT* PSF ($R_{out,opt}$). These are defined as

$$L_{x,FUV} = \int_0^{R_{out,FUV}} I_{FUV}(R) 2\pi R dR \tag{2.7}$$

$$L_{x,opt} = \int_0^{R_{out,opt}} I_{FUV}(R) 2\pi R dR \tag{2.8}$$

where $I_{FUV}(R)$ is the intrinsic light at a radius R and given by

$$I_{FUV}(R) = I_{0,FUV} \ \exp\left(-R/R_{h,FUV}\right). \tag{2.9}$$

Here, $I_{0,FUV}$ is the intrinsic peak intensity and $R_{h,FUV}$ is the intrinsic FUV scale-length obtained from the profile fit. The above relation imply that $\Delta L_x = 0$ when $R_{out,FUV} = R_{out,opt}$. We present the values of ΔL_x in Table 2.2.

2.5 Results and Discussion

2.5.1 Enhanced outer disk star formation in BCDs

We find that most of the BCDs have spatially extended FUV emission beyond their well-resolved optical disks in the *HST*. All these BCDs contain a sufficiently large underlying old LSB disk as evident from the NIR profiles, but it is not spatially larger than the FUV counterparts. The extent of the largest FUV counterparts are larger than their optical ones by a factor of ∼two or more. We are observing such large FUV disks for the first time in distant dwarfs. We also see large FUV clumps beyond the optical boundaries of the BCDs which is an indication of gravitationally unstable disks. We discuss in detail the nature of the clumps and their role in the next chapter. Throughout the text in the thesis, we will be using the BCDs GS3 and GS6 as a representative of the sample and for referring to important estimates from our analyses. The imaging of the BCDs GS3 and GS6 are presented in Figures 2.4 and 2.5.

We perform SBP modelling for 12 out of 14 BCDs in the sample. FUV measurements were not possible in the case of GS8 due to non-detection and GS9 due to being too compact to model. Our modelling reveals shallower intrinsic FUV profiles, in the case of GS3, GS6 (Figure 2.6) and eight others (except GS12 and GS14) as compared to their optical counterparts. This means that they have larger exponential disk scale-length in the FUV as compared to that in the optical ($R_{h,FUV}/R_{h,opt} > 1$). Thus the FUV disks in these BCDs are inherently more extended than the optical and not because of the broadening by the FUV PSF. Also, the outer FUV light fraction, $\Delta L_x > 0$ in 12 of these galaxies (including GS5, a marginal case). GS12 and GS14 have $\Delta L_x > 0$ but $R_{h,FUV}/R_{h,opt} < 1$ (Figure 2.7). Such shallow FUV profiles and excess outer

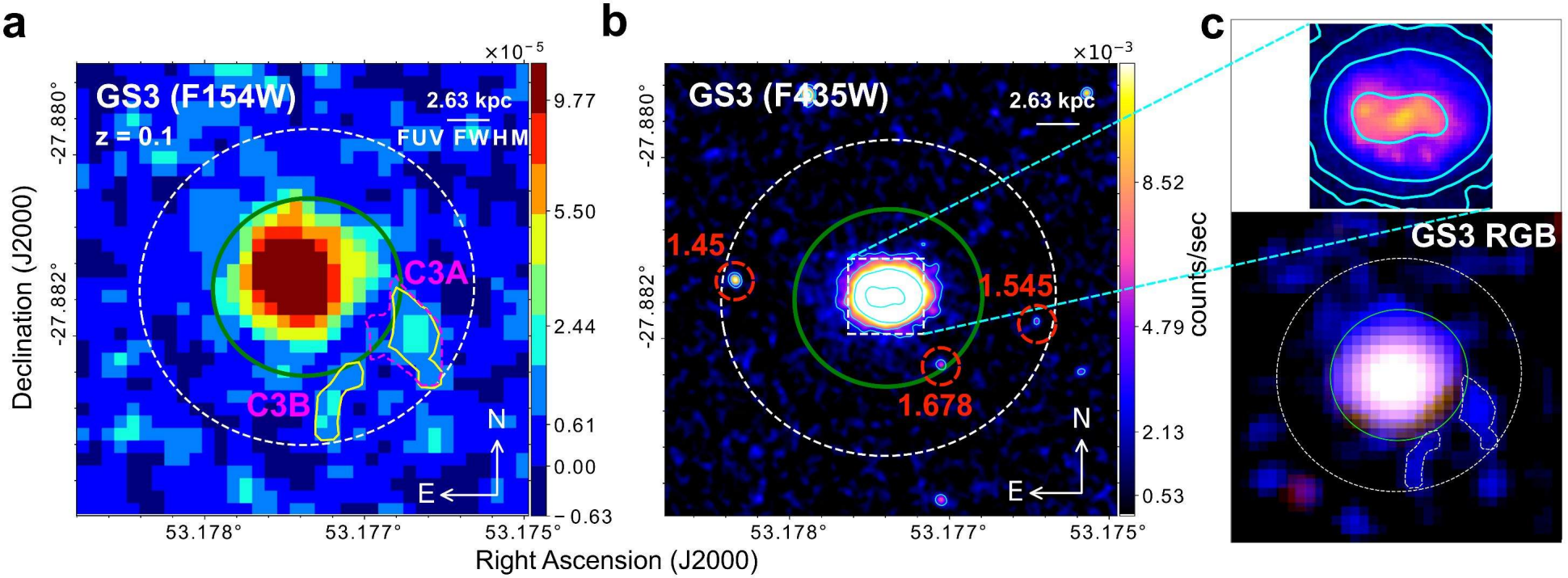

Figure 2.4: **A sample BCD - GS3, showing its size and morphology.** a: False colour image of the BCD - GS3 in F154W band. Detected clumps C3A and C3B present in the XUV regions of GS3 have no optical counterparts. Clumps marked with magenta dashed and yellow solid contours were identified using automated tools. 1 pixel = 0.8 kpc. b: The contours in the *HST*/F435W optical images of GS3 are drawn at 10, 20, 50, 250σ ($\sigma_{GS3} = 3.1\times10^4$ counts/sec/pix). c: Top zoomed-in panel show the inner clumpy structure of GS3 in the optical. The bottom panel is a colour composite image of the BCD made using F154W-band images combined with F435W and F160W blurred by the FUV PSF. For all images, the white dashed ellipse is the FUV extent down to S/N=3 in the measured 1D surface brightness profile and corrected for the width of the PSF by subtraction in quadrature as described in equation 2.5. The green ellipse is the optical extent after the *HST* image is convolved with FUV PSF (marked by solid line in each image) and similarly corrected by subtraction in quadrature. Red dashed circles in the *HST* images mark background galaxies with redshifts from the 3D*HST* catalog[367].

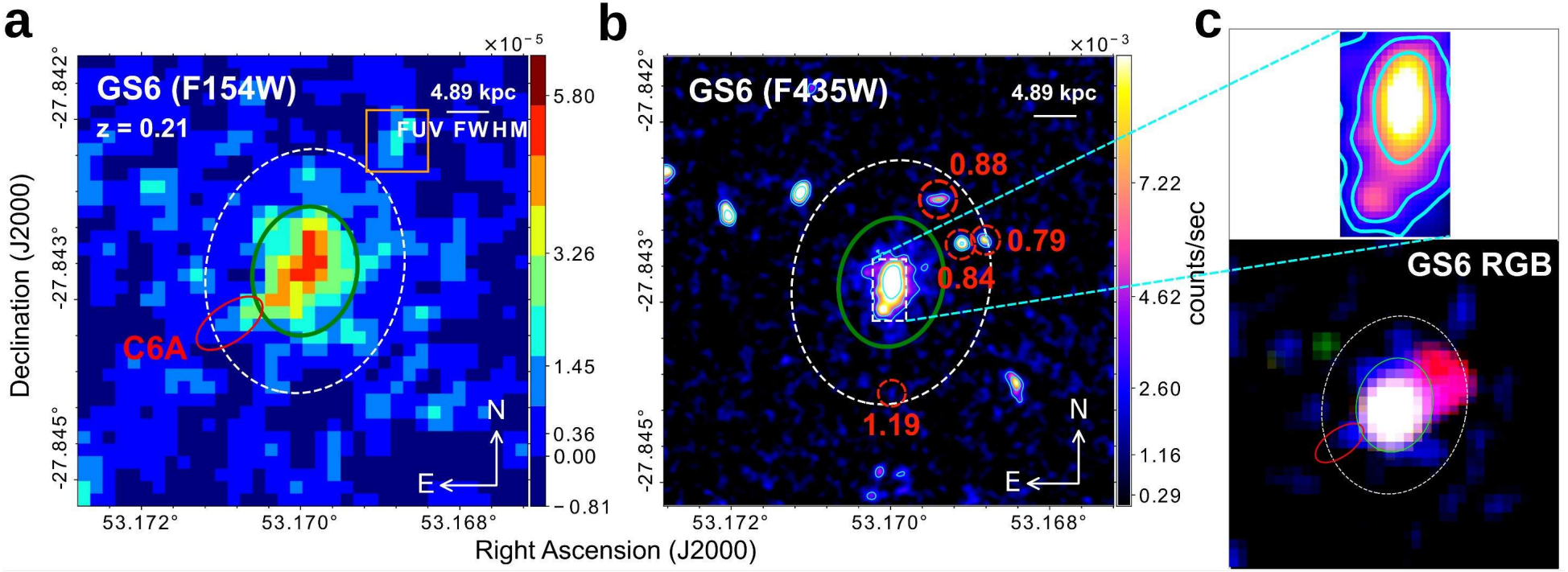

Figure 2.5: **A sample BCD - GS6.** Same as Figure 2.4 but for another BCD - GS6. a: Here, clump C6A in the XUV region has been identified manually. It is marked by a red ellipse. The source marked by the orange box does not have an optical counterpart but is outside the FUV extent of GS6. 1 pixel≃1.4 kpc. b: The contours are again drawn at 10, 20, 50, 250σ levels ($\sigma_{GS6} = 2.9\times10^{-4}$ counts/sec/pix).

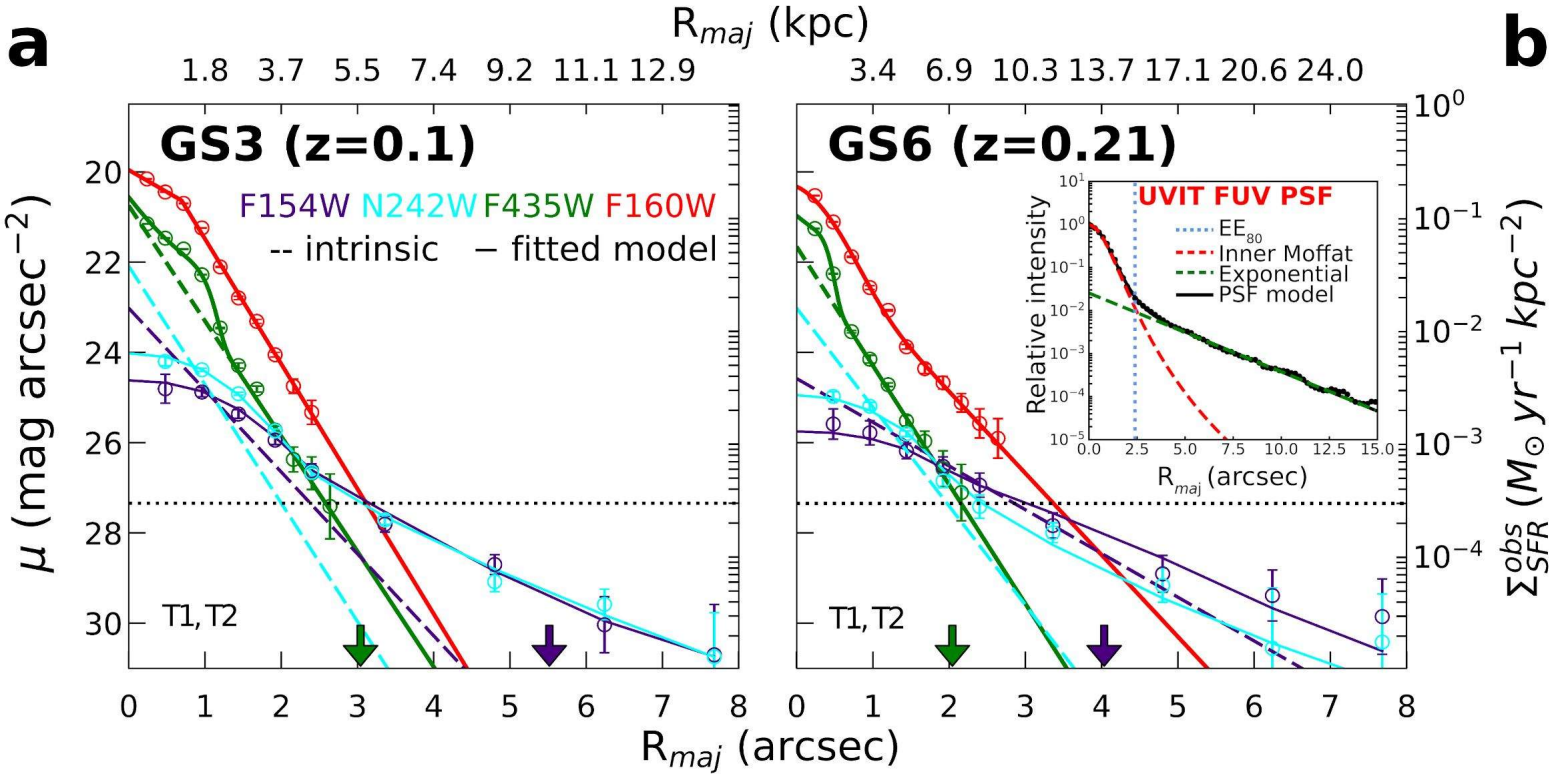

Figure 2.6: **1D surface brightness profile modelling of GS3 and GS6. 1D Surface brightness profile fitting. a, b:** Solid curves show the intrinsic profiles convolved with the PSF as fits to the observed surface brightness. Circles are datapoints in F154W (indigo), N242W (cyan), F435W (green) and F160W (red) bands. The dashed curves in indigo (F154W), cyan (N242W) and green (F435W) represent the fitted intrinsic exponential profiles. The upside down arrows mark the F435W and F154W extents as shown in Figures 2.4 and 2.5. The horizontal dotted line marks the threshold surface brightness level for XUV disks[18]. T1,T2 at the bottom left denotes the XUV disk type[18]. The FUV PSF fit with an inner Moffat profile and an exponential wing is shown as an inset in panel **b**. All surface brightness data points have 1σ error bars. (please refer to section 2.5.2). The surface brightness data points have 1σ error bars.

UV emission suggest extended star formation in cosmically accreting disks. In the case of distant galaxies, where spatial resolution is poor, we can use these parameters to infer the existence of XUV emission. The intrinsic FUV scale-lengths for GS3 and GS6 are ∼1.4 and 2.4 times their respective optical scale-lengths (shown in Table 2.1). In our method to obtain the intrinsic disk scale-lengths, there is an underlying assumption that the BCDs have a single disk component. As we mentioned earlier, this is due to lower UV resolution at these redshifts. Hence assuming multiple components a priori can lead to biases. All derived structural parameters are presented in Table 2.1.

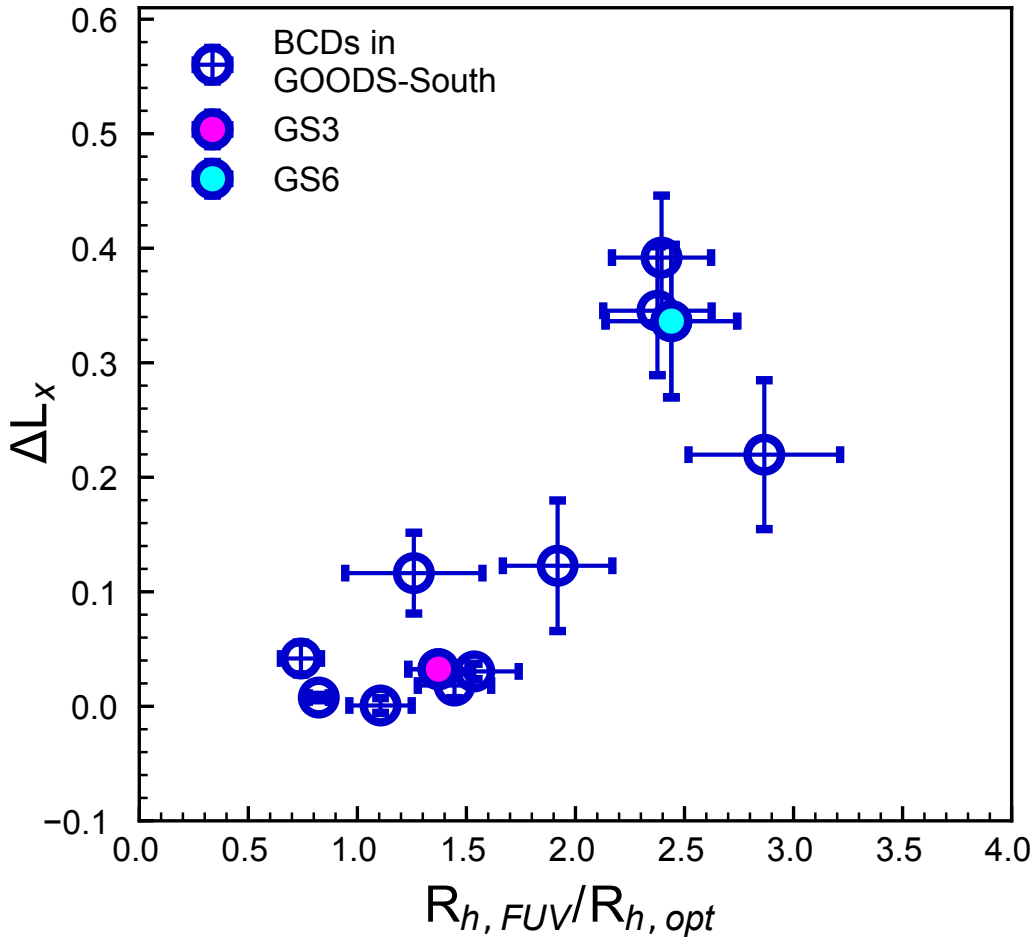

Figure 2.7: **Outer UV light fraction and disk scale-lengths.** The fraction of the total FUV light that is in the XUV disk (defined by the annulus between the optical and FUV extents), ΔL_x, is plotted versus the ratio of the intrinsic, PSF-corrected, FUV-to-optical scale-lengths along with 1σ error bars.

BCD	z	M_{FUV} M_K	$\mu_{0,\,FUV}$ $\mu_{0,\,NUV}$	$\mu_{0,\,opt}$ $\mu_{0,\,nir}$	$\mathbf{r}_{h,FUV}$ $r_{h,NUV}$	$\mathbf{r}_{h,opt}$ $r_{h,nir}$	SFR	FUV-NUV
		mag	mag arcsec^{-2}	mag arcsec^{-2}	kpc	kpc	$M_\odot yr^{-1}$	mag
GS1	0.13	-15.13	23.9±0.3	22.7±0.2	**2.1±0.3**	**1.1±0.0**	0.08±0.00	-0.32±0.11
		-16.97	–	20.5±0.1	–	1.0±0.0		
GS2	0.24	-16.40	24.0±0.2	21.2±0.1	**3.4±0.3**	**1.4±0.1**	0.30±0.02	0.17±0.09
		-18.44	23.2±0.1	21.4±0.6	2.4±0.1	2.0±0.2		
GS3	0.1	-15.47	23.0±0.1	20.7±0.3	**1.1±0.1**	**0.8±0.1**	0.11±0.00	0.18±0.05
		-18.05	22.1±0.1	20.0±0.1	0.7±0.0	0.7±0.0		
GS4	0.15	-15.57	23.7±0.2	22.2±0.8	**1.8±0.2**	**1.4±0.3**	0.13±0.01	0.25±0.08
		-18.81	22.2±0.1	20.9±0.9	1.0±0.1	1.1±0.0		
GS5	0.13	-15.00	23.5±0.3	21.1±0.1	**1.3±0.2**	**1.1±0.0**	0.07±0.00	0.34±0.09
		-19.04	22.3±0.1	19.0±0.1	0.8±0.1	1.1±0.0		
GS6	0.21	-15.87	24.6±0.2	21.7±0.3	**3.4±0.3**	**1.4±0.1**	0.18±0.01	0.04±0.11
		-18.48	23.0±0.1	21.3±0.3	1.5±0.1	2.1±0.1		
GS7	0.23	-16.91	22.5±0.2	21.1±0.1	**2.0±0.2**	**1.4±0.0**	0.47±0.02	0.07±0.09
		-18.18	21.5±0.1	19.7±0.1	1.2±0.1	1.1±0.0		
GS8	0.16			23.96±0.31		2.23±0.23		
		-18.30		19.97±0.07		2.35±0.14		
GS9	0.15			24.43±0.55		1.70±0.46		
		-17.07		22.18±0.08		1.46±0.04		
GS10	0.19	-15.92	24.2±0.2	21.7±0.1	**3.6±0.3**	**1.5±0.1**	0.18±0.01	0.18±0.09
		-18.03	22.6±0.1	21.9±0.8	1.5±0.1	2.1±0.3		
GS11	0.22	-17.96	21.7±0.1	21.1±0.8	**2.4±0.1**	**1.5±0.2**	1.24±0.03	0.31±0.04
		-19.66	20.5±0.1	21.7±0.8	1.5±0.0	2.0±0.0		
GS12	0.08	-15.53	22.5±0.1	21.6±0.1	**1.1±0.1**	**1.3±0.0**	0.11±0.00	0.19±0.04
		-18.43	21.6±0.1	20.2±0.0	0.7±0.0	0.8±0.0		
GS13	0.22	-16.19	24.0±0.2	20.8±0.2	**2.8±0.3**	**1.0±0.1**	0.24±0.01	0.00±0.09
		-18.13	22.3±0.2	19.9±0.2	1.2±0.1	1.1±0.0		
GS14	0.1	-14.99	23.8±0.2	23.1±0.3	**1.5±0.1**	**2.0±0.2**	0.07±0.00	0.68±0.07
		-18.62	21.7±0.1	18.9±0.1	0.7±0.0	1.7±0.1		

Table 2.1: **Photometric and structural parameters of the BCDs.** Column 1: The galaxy IDs. Column 2: The redshifts. Column 3: The K_s and FUV band absolute magnitudes. Column 4 and 5: The central surface brightness values in all four bands - FUV (F154W), NUV (N242W), optical (F435W) and NIR (F160W), corrected for redshift dimming and foreground extinction. Column 6 and 7: The scale-lengths from FUV to NIR; for comparison purposes, if a truncated exponential is used, the outer scale-length is given here. Column 8: The measured total SFRs from the FUV light assuming solar metallicity (these rates are lower by 10% at $0.4Z_\odot$). Column 9: The measured FUV - NUV colours. All quoted uncertainties are 1σ.

2.5.1.1 Sensitivity of profile modelling to background subtraction:

Sky background measurements can greatly influence photometry in the faint outskirts of galaxies. We test this effect by modelling the profiles again which are obtained by subtracting a sky value $\pm 1\sigma$ about the mean sky from the respective images. We also include this sky uncertainty in the error budget of the radial profiles. We find that for nine BCDs, a change in $\pm 1\sigma$ sky results in a change of FUV scale-length up to 20%. In the cases of GS7, GS13 and GS14, the change is 70%. This variation is shown in Figure 2.8.

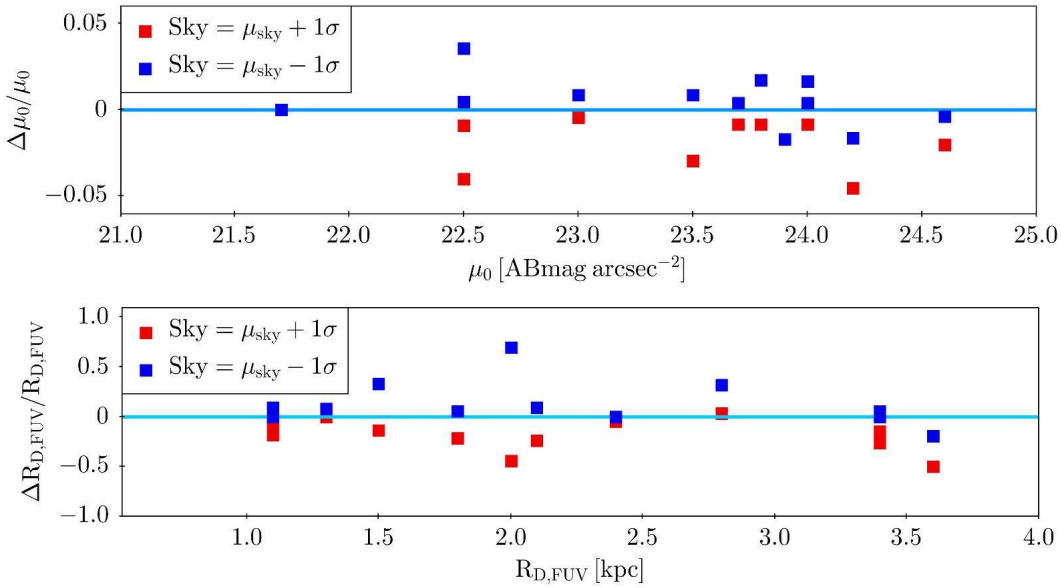

Figure 2.8: **Effect of sky measurement on profile modelling in the FUV band.** Figure shows the variation in the FUV modelled parameters - peak surface brightness (μ_0) and exponential disk scale-length ($R_{D,FUV}$) due to an under/over estimation of FUV sky brightness by 1σ.

2.5.2 Thilker's criteria

We check for the XUV emission in the BCDs using the existing classification scheme constructed for the local galaxies[18]. The foreground, i.e. Galactic extinction corrected[361] FUV surface brightness, corrected for cosmological dimming[368], goes at least as low as ∼28 - 29 ABmag arcsec^{-2}. This is well below the threshold of 27.25 ABmag arcsec^{-2} used as a criterion to define Type 1 XUV disks [18] for local spirals. In our downsized sample of 12 BCDs (except GS8 and GS9), 7 BCDs with outer clumps qualify for T07's Type-1

XUV criteria, 10 of them follow the Type-2 criteria, and 5 of them follow both criteria [18]. The scheme is described as below.

We convert the surface brightness values into the equivalent SFRDs following Kennicutt's SFR calibration[30] at solar metallicity as:

$$SFRD = \frac{1}{A^2} \times 10^{\frac{\mu+48.59}{-2.5}} \times 4\pi D_L^2 \times 1.4 \times 10^{-28}, \quad (2.10)$$

where SFRD is in $M_\odot\ yr^{-1}\ kpc^{-2}$, μ is the surface brightness in mag arcsec^{-2}, A is the angular scale in kpc/arcsec and D_L is the luminosity distance in cm.

The presence of structured UV emission beyond a threshold value of $SFRD_{th} = 3 \times 10^{-4}\ M_\odot\ yr^{-1}\ kpc^{-2} \equiv 27.25$ mag arcsec^{-2} defines a Type 1 XUV disk[18]. Typical sizes of these structures are considered to be ~ 1 kpc in T07's definition. However, at $z \sim 0.1 - 0.24$, the size of a minimum of 4-connected pixels in the FUV image will be in the range of $\sim 1.5 - 3$ kpc. We demonstrate in Figure 2.9 that the outer FUV 'clumps' that we detect in these distant BCDs might be a collection of smaller clumps that appear as a single structure in our *UVIT* observations. At the same time, we may also lose the fainter structures at these redshifts. It is thus challenging to strictly follow the Type-1 definition at these redshifts. But the presence of FUV clumps (which could in fact be a collection of smaller clumps) beyond the detectable optical radii in seven of our BCDs imply that they are Type-1 XUV disks. All the observed FUV profiles of our BCDs reach 27.25 mag arcsec^{-2} and below; beyond the optical radii. On the other hand, Type-2 XUV disks do not necessarily have structured UV clumps but show recent and high star formation activity at large galactocentric radii. Type-2 XUV disks follow the following two criteria[18]:

(i) $FUV - K_s \leq 4$
(ii) $A_{LSB} \geq 7 \times A_{K80}$

where FUV$-$K$_s$ colour is computed in the LSB zone (defined as the area between 'threshold' SFRD contour and the one that encloses 80% of the total flux in K$_s$ band). A_{LSB} is the area of the LSB zone in FUV while A_{K80}

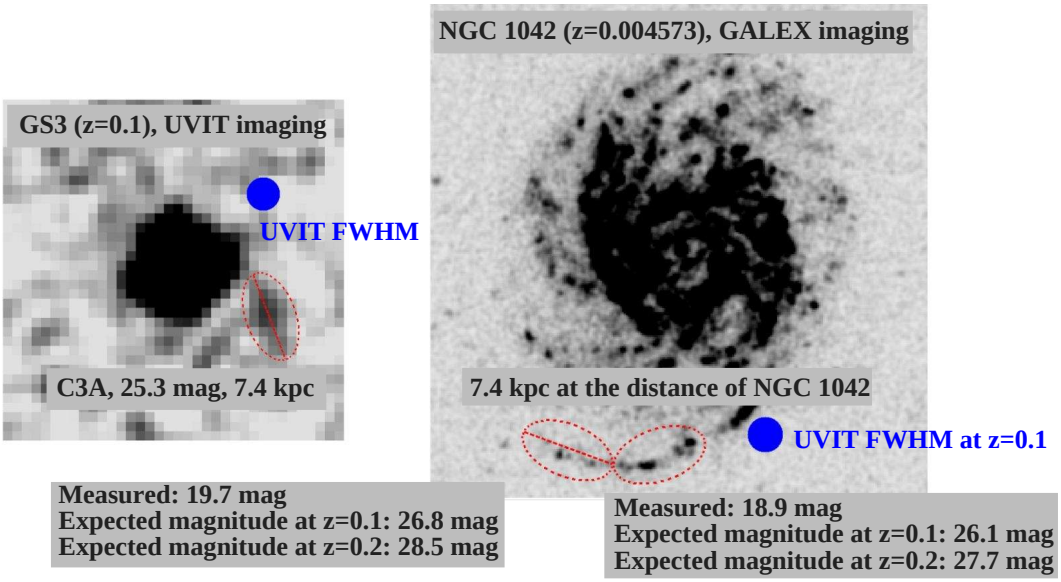

Figure 2.9: **Comparing clumps in GS3 and in the XUV disk galaxy NGC 1042.** On the left is the *UVIT* imaging of GS3 from our sample and on the right is the *GALEX* imaging of a XUV disk galaxy from T07 (NGC 1042). The red ellipses are the ∼size of clump C3A; those overlaid on the *GALEX* image represent the physical size of the clump C3A at the distance of NGC 1042. The same is the case with the *UVIT* FWHM which is overlaid on the *GALEX* image. In terms of angular size, the major axis length of C3A is 4" in the *UVIT* imaging, whereas the major axis length of the ellipses in the *GALEX* imaging is 78.6". This demonstrates that a clump like C3A may in fact be a collection of a number of clumps like those in NGC 1042. Such FUV structures will be very faint at z=0.2. As demonstrated, the brighter collection of clumps in NGC 1042 will be at the 3σ limit of our current *UVIT* observations at z=0.2. Whereas the fainter one will be beyond the limit. Also, by z=0.2 the size of these structures will essentially be equal to *UVIT* FUV-FWHM. Therefore at intermediate redshifts, many outer clumps in a Type 1 XUV disk will go undetected and contribute to the faint diffuse emission of the disk.

refers to the area enclosing 80% of the total flux in K_s band. We refer to the aforementioned XUV disk criteria as 'Thilker's criteria' throughout the text. In order to check whether our BCDs follow Type-2 criteria, we consider the LSB zone's outer radius to be $R_{out,FUV}$. The K_s band PSF has an FWHM of ∼0.4 arcsec[305] that makes it better than the FUV PSF by more than a factor of 3. We compute the FUV-r colour by degrading the intrinsic FUV models with the PSF of K_s band imaging. We find that GS3 ($FUV - K_s$ = 1.25, $A_{LSB} = 16.9A_{K80}$), GS6 ($FUV - K_s = 0.56$, $A_{LSB} = 7.2A_{K80}$) and eight others, i.e., a total of 10 BCDs, satisfy Type-2 XUV criteria. Finally, 11 BCDs in our sample host either Type-1 or Type-2 XUV disks or both based on Thilker's criteria. The various metrics derived for the purpose of XUV disk

BCD	$M_{*,total}$	$M_{*,young}$	FUV-K_s	$\frac{A_{LSB}}{A_{K80}}$	XUV	ΔL_x
	log $M_\odot$	log $M_\odot$	mag		Type	%
GS1	8.13	7.4	0.08	17.6	T1,T2	12.3±5.7
GS2	8.73	8.12	-0.03	13.4	T2	34.5±5.6
GS3	8.57	7.83	1.25	16.9	T1,T2	3.2±0.1
GS4	9.02	7.9	1.53	15.0	T2	11.6±3.5
GS5	8.92	7.87	3.24	6.5	–	0.1±0.1
GS6	8.65	7.6	0.56	7.2	T1,T2	33.6±6.7
GS7	8.70	8.43	-0.87	34.1	T2	1.8±1.1
GS10	8.48	7.74	-0.41	10.3	T1,T2	39.2±5.4
GS11	8.99	8.69	-0.01	22.2	T2	3.0±0.1
GS12	8.66	7.57	3.68	6.1	T1	0.1±0.0
GS13	8.59	8.07	-0.61	20.1	T1,T2	21.9±6.4
GS14	8.73	8.02	2.17	14.0	T1,T2	4.2±1.4

Table 2.2: **Various metrics derived for the XUV disks of the BCDs. Column 2:** Total stellar mass of the galaxy. **Column 3:** Young stellar mass of the galaxy. **Column 4, 5:** FUV-K_s colour and fraction of LSB area measured to check for Type 2 XUV disk. **Column 6:** Type of XUV disk as per Thilker's criteria, Type-1 (T1) and Type-2 (T2). **Column 7:** FUV fraction in XUV region. The quoted uncertainties are 1σ.

classification is presented in Table 2.2. We present the complete BCD sample along with their profile modelling in Appendix of this chapter.

2.5.3 Gas accretion rates

As we discussed in Chapter 1 and in section 2.1, XUV disks are a possible manifestation of gas infall from the surrounding medium. All BCDs in our sample appear to be non-interacting, with the possible exception of GS11 and GS13. So we assume that cold gas accretion from the environment is fueling their XUV disks. We derive gas accretion rates in the XUV regions following the prescription of Fraternali & Tomassetti (2012)[369]. We first convert the model FUV luminosities into star-formation rates using the following relation from Kennicutt 2012[30]

$$SFR(M_\odot\ yr^{-1}) = 1.4 \times 10^{-28}\ L_\nu(ergs\ s^{-1}\ Hz^{-1}) \tag{2.11}$$

Assuming a constant star-formation history (SFH) in these regions, equation 13 in Fraternali & Tomassetti (2012)[369] reduces to a simpler expression for

the instantaneous gas accretion rate as follows:

$$\dot{M} = (1 - \mathcal{R}) \times SFR \tag{2.12}$$

where $\mathcal{R}$ is the return factor which is an estimate of the fractional mass the stars return to the ISM. We use a value of $\mathcal{R}$=0.3 that is also commonly used for the MW and external galaxies as discussed in Fraternali & Tomassetti (2012)[369]. This value depends on the IMF which is considered to be Salpeter[370] here. We calculate the instantaneous accretion rate for all the XUV disks of the BCDs discussed in this work. The mean of all the instantaneous accretion rates is 9.37 $\times$ 10^{-2} $M_{\odot}yr^{-1}$. Our mean gas accretion rate onto the BCDs is comparable to the lower limit of accretion rates $\sim$0.1–0.2 $M_{\odot}$ yr^{-1} derived based on the HI measurements and to sustain the SFR in local disk galaxies[371]. However, note that this simpler expression (equation 2.12) has many caveats: the unknown SFH, actual reprocessing factor of stellar material, star-formation timescale, gas/stellar densities, ISM turbulence.

2.6 Summary and Conclusions

We analyze multi-wavelength imaging observations from FUV to NIR of a sample of intermediate redshift BCDs (0.1$\leq$z$\leq$0.24). New wide-field and deep FUV observations using the *UVIT*[6] onboard *AstroSat*[7] is used in this study which has a factor of $\sim$3 better spatial resolution than *GALEX*. This provides us with the advantage of detecting fainter structures and obtaining better FUV radial profiles. We obtain 1D radial surface brightness profiles of the BCDs and based on a criteria of S/N = 3, we find that most of them are spatially extended in the FUV as compared to their optical counterparts. The deep FUV imaging also reveal clumpy structures beyond their optical boundaries which do not possess a counterpart in the HST imaging. *UVIT's* resolution is well suited to resolve massive, outer FUV clumps in Type 1 XUV disks up to intermediate redshifts of $\sim$0.1 or so. *UVIT's* FWHM of $\sim$1.4"[358] translates to a resolvable clump size of 2.6 kpc at this redshift (in case of *GALEX's* FUV FWHM of 4.5" it is 8.3 kpc). At the same time, the bigger FoV of *UVIT* is an advantage over the *HST*-FUV observations. For example in this case,

though we have higher resolution FUV observations for the *GOOD-South* field from *HST*, the coverage is very limited as compared to that of our *UVIT* observations. Hence, we are able to study all the (redshift limited) BCDs in the field. The model the 1D radial profile across all UV-optical-NIR bands (*UVIT* and *HST*) and obtain intrinsic PSF corrected disk scale-lengths. We find that 10 BCDs have larger FUV scale-lengths as compared to their optical ones and their FUV light fraction beyond the optical boundaries is greater than zero. These findings imply that these BCDs host XUV disks which is a common building mechanism in nearby spirals. Such XUV disks have not been reported earlier in distant BCDs. Our XUV claims are substantiated by previous XUV disk criteria from T07. As previous studies suggest that the presence of XUV disks often indicates a conversion of accreted peripheral cold gas into stars, our intermediate-z BCDs may very well be growing their stellar disks in this manner. This can be confirmed by using high-resolution HI observations in the future with facilities such as the Square Kilometre Array (SKA).

Appendix

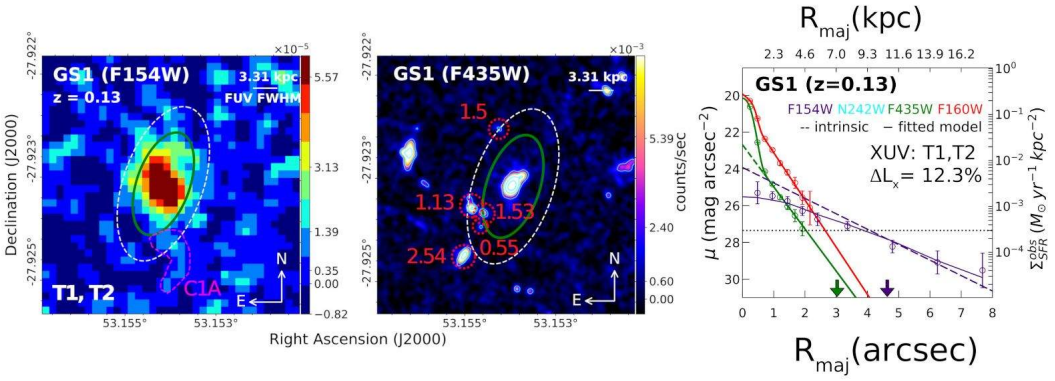

Figure 2.10: **Sample BCD: GS1**

Figure 2.10 (GS1): With an XUV light fraction, $\Delta L_x > 0$ and FUV scale-length > optical scale-length, this BCD hosts an XUV disk. This BCD displays an FUV clump outside its optical extent and qualifies both as a Type 1 and Type 2 XUV disk as per T07. It is interesting to note that the apparent position angles of the optical and UV disks are different. We find this misalignment only in the FUV imaging. There may be young unresolved structures in

that region resulting in the apparent position angle of the UV disk. However, we lack the necessary observations to confirm this at this stage.

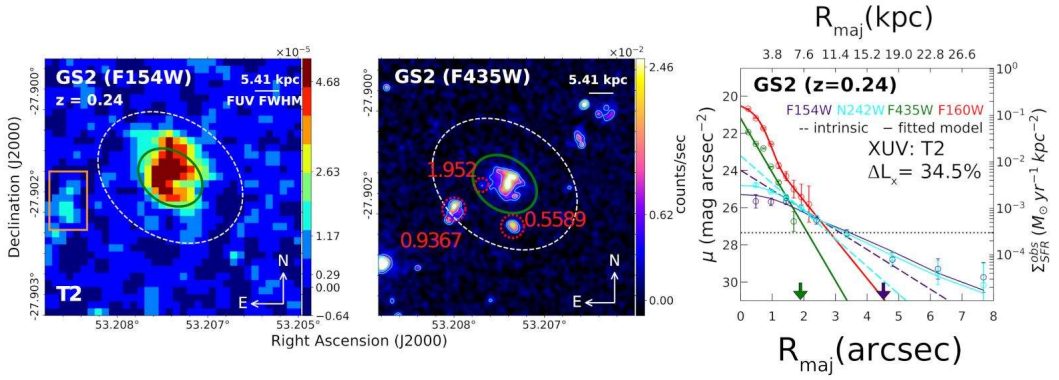

Figure 2.11: **Sample BCD: GS2**

Figure 2.11 (GS2): This BCD hosts an XUV disk. But it does not show any discrete FUV structure outside the optical extent and hence do not qualify as Type 1 XUV disk. But it qualifies as a Type 2 XUV disk as per T07. Towards the east we mark a FUV detection having S/N> 3 but without any visible HST counterpart.

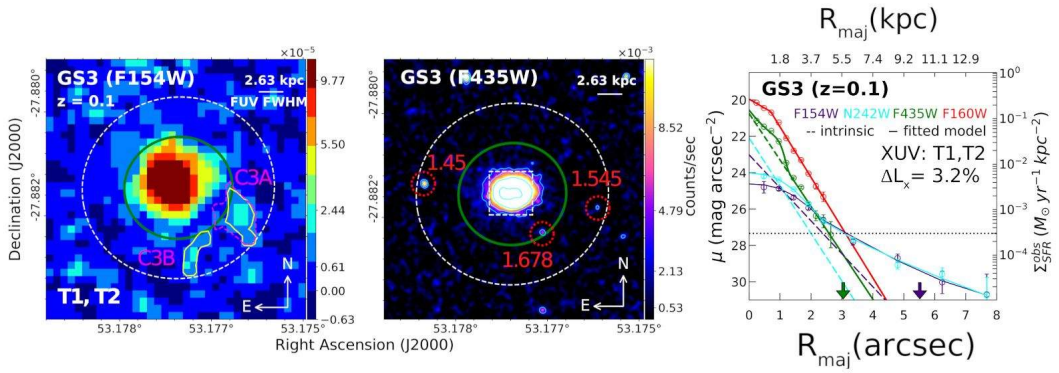

Figure 2.12: **Sample BCD: GS3**

Figure 2.12 (GS3): This BCD with an XUV disk is one of our best representatives of the sample. This contain two clump outside the optical extent qualifying as a Type 1 XUV disk. This also qualifies to be a Type 2 XUV disk as per T07.

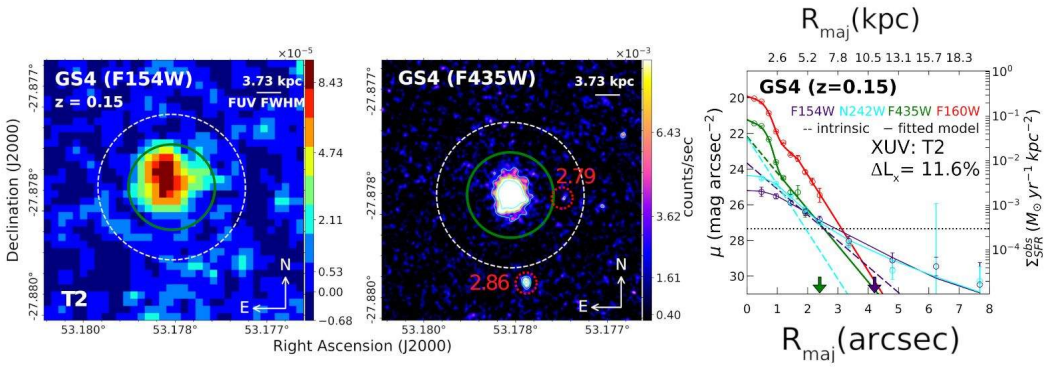

Figure 2.13: **Sample BCD: GS4**

Figure 2.13 (GS4): This BCD with an XUV disk qualifies as a Type 2 XUV disk as per T07.

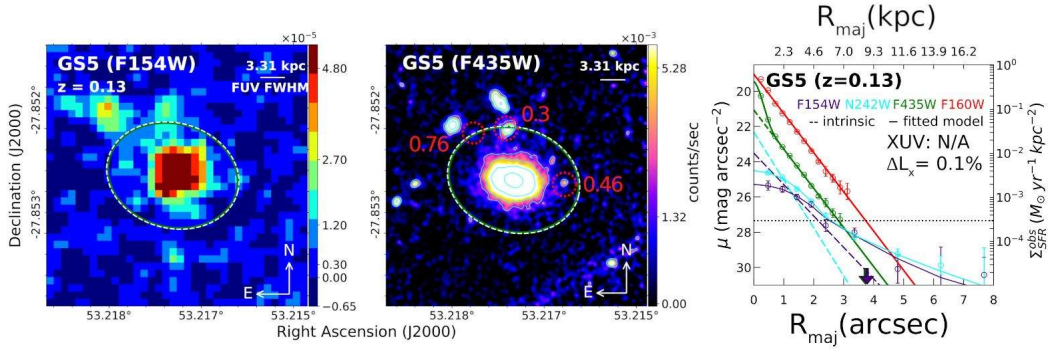

Figure 2.14: **Sample BCD: GS5**

Figure 2.14 (GS5): This BCD is a marginal case of XUV disk. The XUV region is marginal which contains negligible FUV light. It do not qualify as a Type 1 or Type 2 XUV disk as per T07.

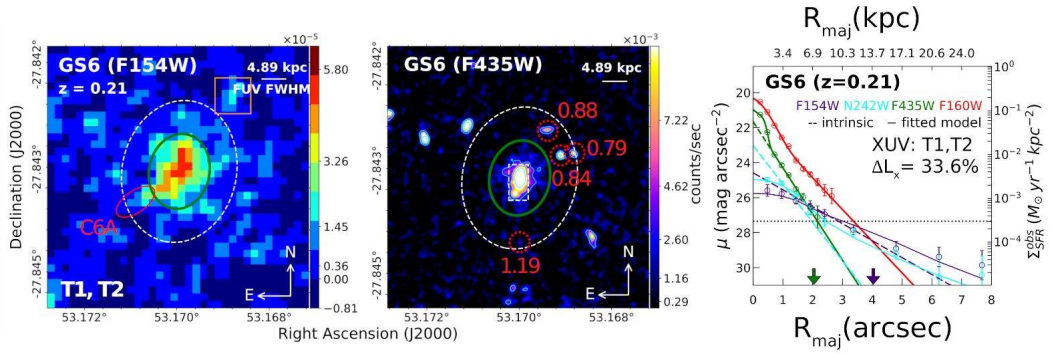

Figure 2.15: **Sample BCD: GS6**

Figure 2.15 (GS6): This BCD with an XUV disk is one of the best representatives of our sample. This contains clump outside the optical extent qualifying

as a Type 1 XUV disk. At the same time it contains a high XUV light fraction. This BCD also qualifies as a Type 2 XUV disk as per T07. Towards the north-west direction is an FUV detection (S/N>3) without an HST counterpart, but this is outside the FUV extent so we consider it as part of the BCD.

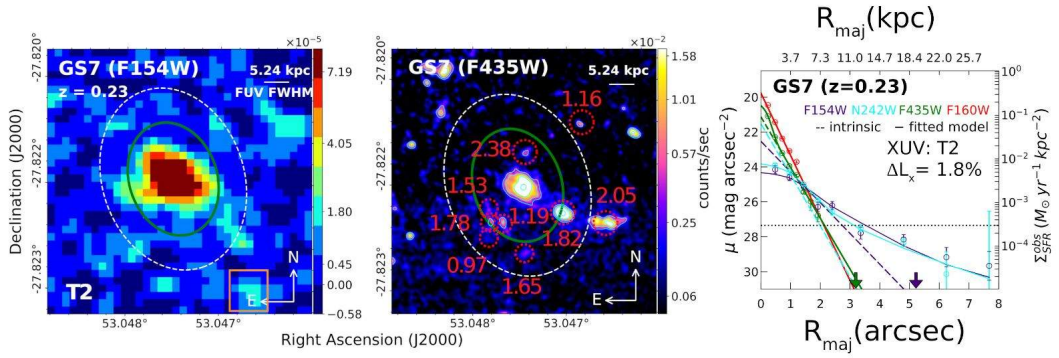

Figure 2.16: **Sample BCD: GS7**

Figure 2.16 (GS7): This BCD with an XUV disk qualifies as a Type 2 XUV disk as per T07.

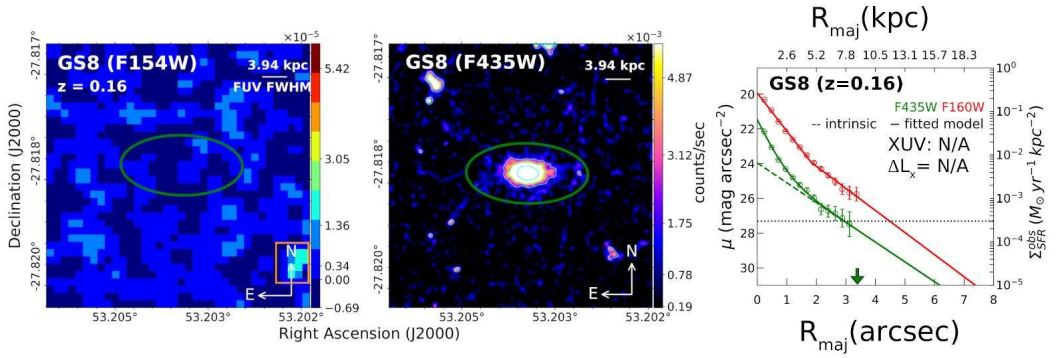

Figure 2.17: **Sample BCD: GS8**

Figure 2.17 (GS8): It is interesting to note that this BCD is not detected in the FUV. Usually, BCDs are characterized by their central star formation.

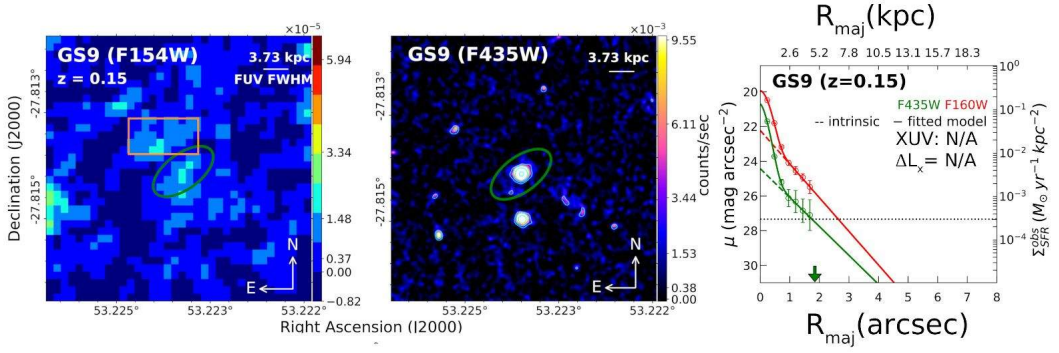

Figure 2.18: **Sample BCD: GS9**

Figure 2.18 (GS9): This BCD is too compact in the FUV to perform reliable modelling. So we avoid it from the analysis. Towards its northeast direction, there is an FUV detection (S/N>3) and without HST counterpart. With current observations used in this analysis, we cannot confirm its association with the BCD.

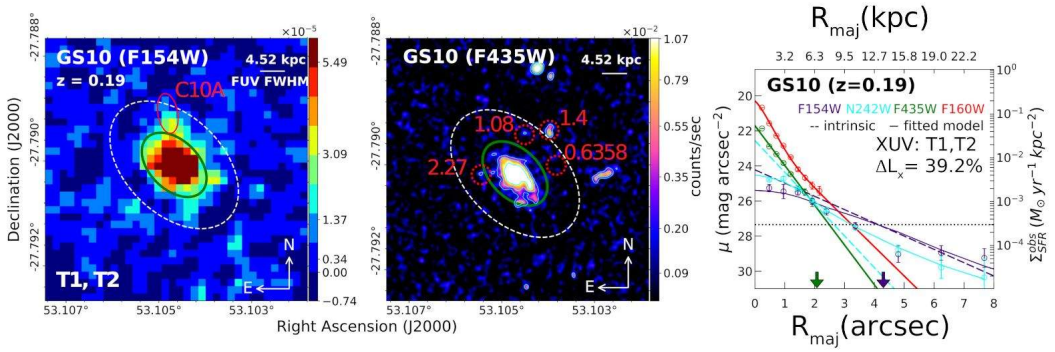

Figure 2.19: **Sample BCD: GS10**

Figure 2.19 (GS10): This BCD with an XUV disk qualifies as both a Type 1 and Type 2 XUV disk as per T07. It also contains the highest fraction of XUV light fraction.

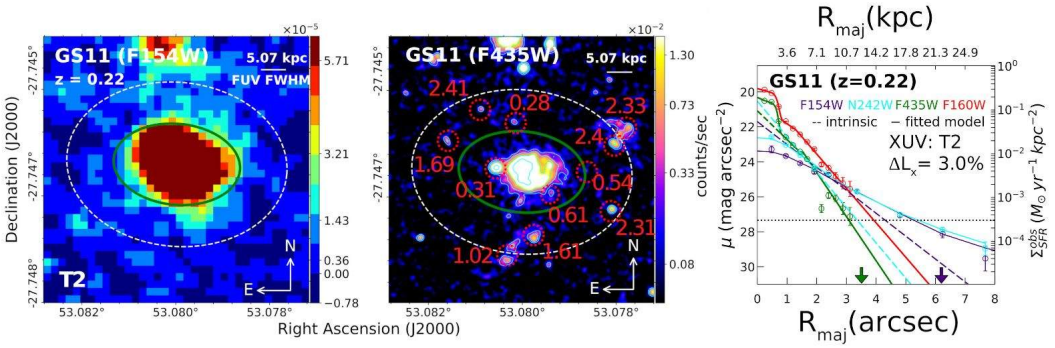

Figure 2.20: **Sample BCD: GS11**

Figure 2.20 (GS11): This BCD with an XUV disk qualifies to be a Type 2 XUV disk as per T07.

Figure 2.21 (GS12): This BCD has negligible XUV light fraction and FUV scale-length < than the optical scale-length. But we find FUV clumps beyond the optical extent. This BCD qualifies as a Type 1 XUV disk as per T07.

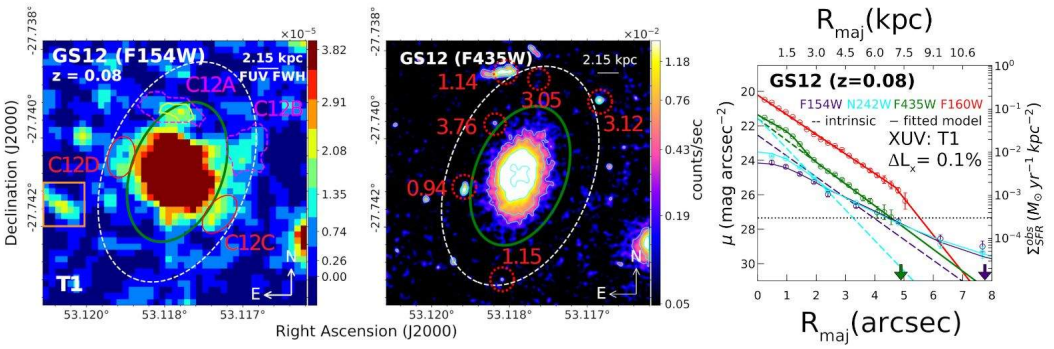

Figure 2.21: **Sample BCD: GS12**

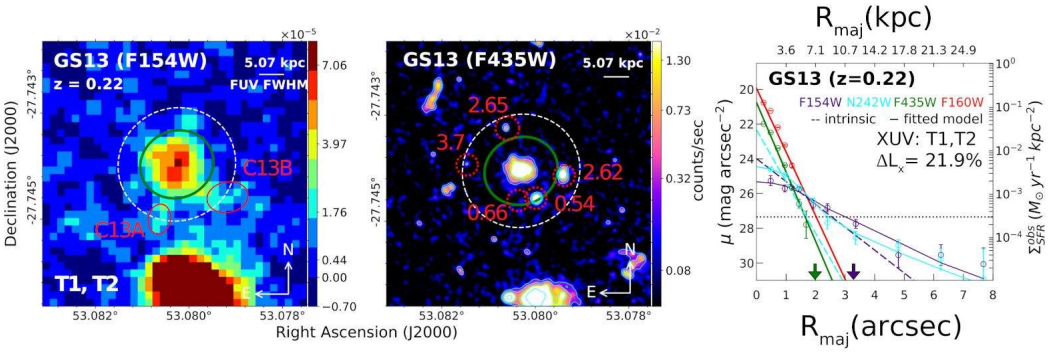

Figure 2.22: **Sample BCD: GS13**

Figure 2.22 (GS13): This XUV disk BCD qualifies as both a Type 1 and Type 2 XUV disk as per T07. It has a bright companion nearby (GS11). Based on the redshift of these objects, there is a possibility of interaction.

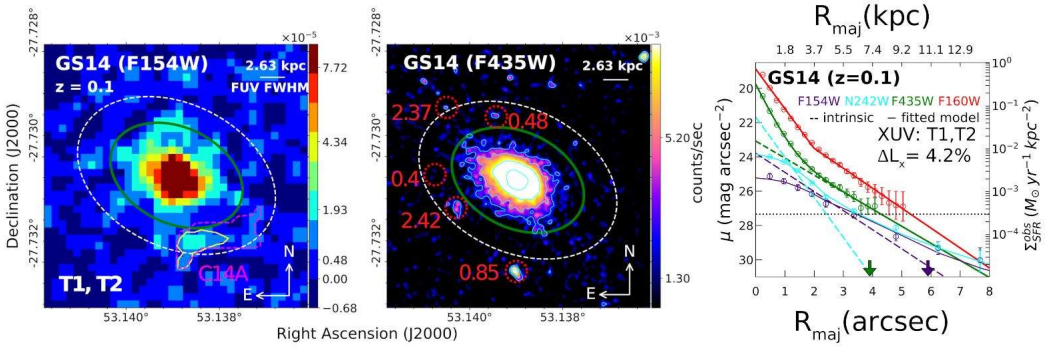

Figure 2.23: **Sample BCD: GS14**

Figure 2.23 (GS14): Like GS12, this BCD also has FUV scale-length < optical scale-length. But we find FUV clumps beyond the optical extent. This BCD qualifies as both a Type 1 and Type 2 XUV disk as per T07.